Surface oxidation of Permalloy thin films

M. R. Fitzsimmons,[1] T. J. Silva,[2] and T. M. Crawford[1,*]
[1]*Los Alamos National Laboratory, Los Alamos, New Mexico 87545, USA*
[2]*National Institute of Standards and Technology, Boulder, Colorado 80303, USA*
(Received 1 April 2005; revised manuscript received 6 October 2005; published 24 January 2006)

The chemical and magnetic structures of oxides on the surface of Permalloy $Ni_{81}Fe_{19}$ films were investigated as functions of annealing time with x-ray and polarized neutron reflectometry. For annealing times of less than one hour, the oxide consisted of a 1.5-nm-thick layer of NiO on an Fe oxide layer that was in contact with Permalloy. The Fe oxide thickness increases with annealing time with a parabolic rate constant of 10^{-18} cm^2 s^{-1} (for an annealing temperature of 373 K). The growth of the oxide layer is limited by the rate at which oxygen appears below the NiO layer. No portion of the oxide region was found to be ferromagnetically ordered for films annealed less than one hour. The growth of the Fe oxide region is well correlated with the measured increase of the second-order magnetic susceptibility for similarly prepared samples.

DOI: 10.1103/PhysRevB.73.014420 PACS number(s): 75.70.Ak, 75.70.Cn, 61.12.−q, 61.10.−i

I. INTRODUCTION

Permalloy ($Ni_{81}Fe_{19}$) is a canonical soft alloy ferromagnet, having seen use in multiple applications from transformer cores to magnetic recording heads, and is a candidate component material for future spintronic devices. In addition to its magnetic robustness, Permalloy's ability to resist corrosion also makes it a standard to which other materials should be compared for magnetic device applications in various environmental conditions. Corrosion resistance is imparted by the formation of a passivation layer on the surface of a Permalloy film upon exposure to air, which is reminiscent of the corrosion resistance of Al. Corrosion resistance can be enhanced through the intentional growth of the surface passivation layer by annealing in an oxygen-rich atmosphere.[1]

Nonlinear optical studies of magnetic materials, including Permalloy, exhibit a magnetic contrast mechanism analogous to the linear magneto-optic Kerr effect in second-harmonic generation (SHG). The second-harmonic magneto-optic Kerr effect (SH-MOKE) exhibits both enormous contrast and interfacial sensitivity.[2,3] The interfacial sensitivity is derived from the absence of symmetry at an interface between dissimilar materials. SHG can also be produced in bulk materials from magnetic-dipolar interactions between the laser light and the material,[4] or by electric-dipolar interactions in materials lacking a center of symmetry.[5] Since Permalloy is a center-symmetric material, electric-dipole production is forbidden.[6] Nevertheless, Permalloy[5] films exhibit an easily detected SH-MOKE signal.[7] In transverse *p*-incidence geometry, the SHG efficiency of a film is found to vary linearly with the component of the magnetization transverse to the plane of incidence.[8] Contrast in the *p*-transverse geometry is approximately 60% for Permalloy.[9]

Previously, the annealing of Permalloy films under conditions of low humidity and moderate heat (373 K) was found to greatly enhance second-harmonic generation compared to unannealed (virgin) films.[10] Annealing times of less than 1 h resulted in a monotonic increase in the average level of SHG, while its absolute change due to magnetization reversal was unaffected. After a 1 h anneal, the level of SHG in the absence or presence of a magnetic field decreased in amplitude. These observations seem to suggest two sources of SHG, one scaling with film thickness (a bulk effect) and the other related to an interface between nonmagnetic and magnetic materials.

An x-ray and polarized neutron reflectometry study was undertaken to determine likely origins of SHG from annealed Permalloy films and the passivation of Permalloy.[1] Both techniques are nondestructive and probe the depth profile of the scattering potential of a sample averaged over its lateral dimensions.[11] The x-ray scattering potential is purely chemical, whereas that for polarized neutron reflectometry consists of nuclear (chemical) and magnetic components.[12–15] By observing how annealing influences periodic features of the x-ray and neutron reflectivities, we determine the chemical-magnetic structure depth profiles of the samples as a function of annealing time, and show that the presence and growth of an Fe oxide layer is likely responsible for increases of second-harmonic generation in similarly prepared samples.

II. SAMPLE PREPARATION

Polycrystalline Cu films 50 nm thick were deposited onto 7.6-cm-diameter (001) Si substrates using planar magnetron sputtering followed by deposition of 50-nm-thick polycrystalline films of Permalloy ($Ni_{81}Fe_{19}$). The depositions were made at room temperature at rates less than 1 nm/s. The wafer was cleaved into several 2×2 cm^2 pieces. One piece, sample A, was reserved so that measurements of a sample in the unannealed condition could be made. Five other pieces were placed on a hot plate previously heated to 373 ± 3 K in an environment with an absolute humidity of 3.36 ± 0.34 g/cm^3. After annealing for 300 ± 5 s sample B was removed from the hot plate. After an additional 600 ± 5 s, sample C was removed and so forth. The samples were annealed for the times reported in Table I. A schematic diagram of a typical sample is shown in Fig. 1.

TABLE I. Preparation characteristics of the samples and oxide layer thickness (deduced from reflectometry).

Sample	Annealing time (s)	Oxide layer thickness Δ (nm)
A	0	2.6±0.1
B	300±5	2.7±0.1
C	900±5	2.9±0.1
D	3600±5	3.2±0.1
E	19380±5	6.6±0.1
F	68400±5	7.4±0.1

In order to relate measurements of oxide surface layer thicknesses obtained from x-ray and neutron reflectometry to the annealing time dependence of SHG, we prepared a second set of samples for study with SH-MOKE. These samples differ from those studied with x-ray and neutron reflectometry in that the Permalloy film layer was 100 nm thick (rather than 50 nm), and they were annealed at a temperature of 503 K (rather than 373 K).

III. RESULTS

After annealing, each sample was examined with x-ray reflectometry. In addition to the x-ray measurements, samples A, E, and F were studied with polarized neutron reflectometry. Reflectometry involves measuring the intensity of the specularly reflected radiation through an angle 2α

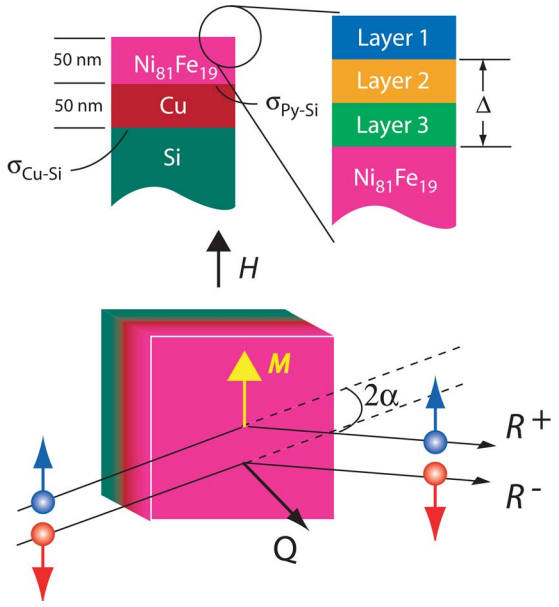

FIG. 1. (Color online) Upper: Cross section of a sample represented by a three-layer oxide, Permalloy, Cu, and Si. The thickness of the second and third layers is Δ. The roughness or interdiffusion of an interface is described by an error function whose derivative, a Gaussian function, has a root-mean-square width of σ. Lower: A spin-up (blue) or spin-down (red) neutron is reflected through the angle 2α by the sample surface. The x-ray scattering experiment is conceptually similar.

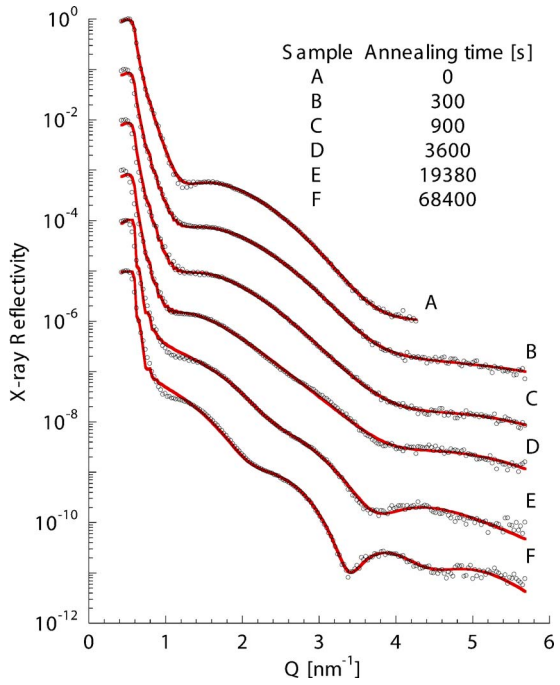

FIG. 2. (Color online) X-ray reflectivities for the samples. The reflectivities are displaced (in the vertical direction) for the sake of clarity. The solid curves are reflectivities calculated from models fitted to the data (see text).

(Fig. 1), and comparing this intensity to the intensity of the radiation illuminating the sample. The ratio, called the reflectivity R, is measured as a function of wave-vector transfer $Q=4\pi \sin(\alpha)/\lambda$, where λ is the wavelength of the radiation.

The x-ray reflectivities for the different samples are shown in Fig. 2 after removal of the instrumental background. The periods of the modulation of R with Q are related to the thicknesses of the oxide layers. The amplitude of the modulation and the attenuation of R with Q are related to the change of electron density and roughness, respectively, of the almost planar interfaces near the sample surface.

The polarized neutron reflectivities of three samples are shown in Fig. 3, after removal of the instrumental background and correction for polarization efficiencies.[16] The large difference between the non-spin-flip reflectivities (corresponding to the intensities measured for fixed incident and reflected neutron polarization, either both spin up R^+ or both spin down R^-) is related to the component of the vector magnetization $M_\parallel$, parallel to the 79.6 kA/m (1 kOe) field H, applied in the plane of the sample and perpendicular to the direction of the incident neutron beam and Q. In addition to information about the nuclear depth profile of the sample, information about ferromagnetism, i.e., the magnetic depth profile, can be deduced from differences between R^+ and R^- as a function of Q.

For the SH-MOKE study, data were taken in the transverse p orientation: The incident fundamental light was p polarized, with the applied magnetic field axis perpendicular to the plane of incidence. A Ti:sapphire pulsed-laser source was used, with a focused spot size of ~90 μm. Details of the experimental configuration have been previously reported.[9] The average optical power of SHG from the sample's surface

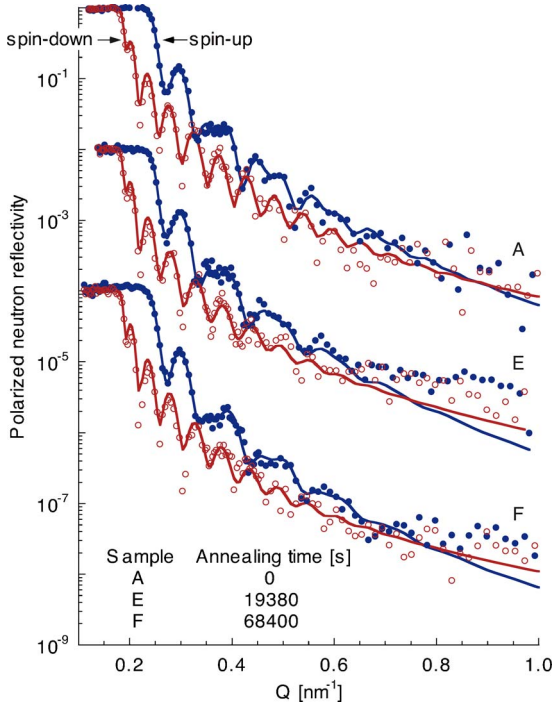

FIG. 3. (Color online) Polarized neutron reflectivities (●, spin up, and ○, spin down) for samples A, E, and F. The reflectivities are displaced (in the vertical direction) for the sake of clarity. The blue (spin-up) and red (spin-down) curves were obtained from models fitted to the data.

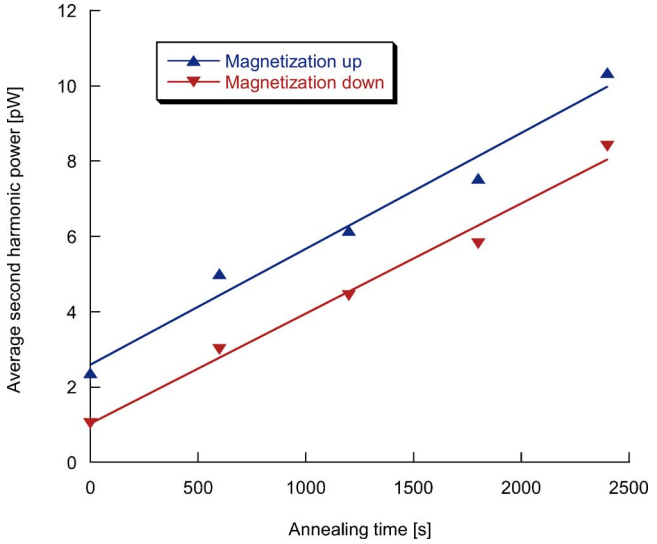

FIG. 4. (Color online) Average optical power of second-harmonic generation from the sample for oppositely saturated magnetization directions in the *p*-incidence, transverse magnetization geometry. Dashed and dotted lines are the results of linear regression to the data. The average slope of the two lines is 0.003 pW/s of annealing at 503 K, with an average initial second harmonic yield of 1.7 pW.

was measured for oppositely saturated magnetization directions in the *p* incidence, transverse magnetization geometry (Fig. 4). The magnetic contribution to the SHG is related to the difference between the magnetization "up" and "down" signals. This difference is unaffected by annealing at 503 K for times less than 2500 s. However, the average signal, which is related to a nonmagnetic source of SHG, increases dramatically and linearly with time.

IV. DISCUSSION

In order to obtain the chemical and magnetization depth profiles of the annealed samples, the reflectivities of model film structures were calculated and compared to the observed x-ray and neutron reflectivities. We used a model that treats the film as a sequence of layers (e.g., those in Fig. 1). Each layer had its own index of refraction[17] $n=1-\lambda^2\rho_e r_e/2\pi - i\zeta\lambda/4\pi$, where ρ_e is the average electron density of the layer with units of e^- per nm^3 (equal to the sum over the number density N of atoms with atomic number Z), r_e is the classical electron radius (2.82×10^{-6} nm), and ζ is the linear absorption coefficient. Here, the product $\rho_e r_e$ is the x-ray scattering-length density β_x (nm^{-2}) of a given layer.

In the case of polarized neutron reflectometry, the scattering-length density β is a combination of nuclear β_n and magnetic β_m components.[12–14] The nuclear component is the product of N and the neutron scattering length b of the atom or molecule. The magnetic component of the neutron scattering-length density is the product of a constant C $=2.645\times10^{-6}$ nm/μ_B and the net magnetic moment of the atoms or molecules μ, averaged over the lateral dimensions of the sample in the direction of the magnetizing field such that $\beta_m=\pm C\mu N$. The positive sign is used to compute the spin-up scattering-length density and the negative sign the spin-down scattering-length density. Since the x-ray, and neutron scattering-length densities are both proportional to the atomic (or molecular) density N, determination of β_x and β_n can be used to identify the chemical composition of the sample (averaged over its lateral dimensions) as a function of depth. Since electron density and nuclear scattering lengths are uncorrelated, information related to these quantities can help identify the composition of a material. For example, there are at least 25 compounds containing different combinations of Fe, Ni, O, and H, and by comparing information from the x-ray and neutron scattering experiments (discussed later), the composition of the annealed Permalloy surface layers can be reduced to only four candidates (and in one instance the composition of an oxide layer was uniquely identified).

In addition to its scattering-length density, a layer is characterized by its thickness Δ and the roughness or interdiffusion across interfaces between layers. Roughness (or interdiffusion) across an interface was treated by connecting the scattering-length density of one layer to another via an error function density profile[11] that has a Gaussian derivative with root-mean-square width of σ. The scattering-length-density depth profile is calculated for a sequence of layers, which serves as the basis for determining the chemical and magnetization depth profiles across the Permalloy samples. A recursive optical reflection and refraction algorithm was applied to the scattering-length-density profile to calculate its x-ray and polarized neutron reflectivities using the Parratt

TABLE II. X-ray and neutron scattering-length densities and magnetizations obtained for the layers representing the sample oxide.

	β_x (10^{-3} nm^{-2})	β_n (10^{-4} nm^{-2})	Ms (kA/m)
	Samples A–D		
Layer 1 (not observed)			
Layer 2 (NiO)	5.4±0.2	8.7±0.3	0±105
Layer 3 (α-Fe_2O_3 or FeO)	4.6±0.2	7.5±0.2	0±105
	Samples E and F		
Layer 1 (Ni-Fe oxyhyrodroxide or oxyhydrate)	1.5±0.5	2.0±0.5	0±105
Layer 2 (reduced NiO)	6.7±0.3	9.5±0.2	0±105
Layer 3 ($NiFe_2O_4$+Permalloy)	6.0±0.5	8.6±0.5	877±105

formalism.[11] The parameters of the profile, i.e., Δ, β_x, β_n, β_m, and σ (results are shown in Tables I–III), were adjusted until a measure of error was minimized. The measure of error χ^2 was chosen to be the sum of the logarithms of the squared differences between the calculated R^{calc} and observed R profiles (whether x-ray or neutron) normalized to the variance δR_i^2 of the measurement, i.e., $\chi^2=\Sigma_i \ln[(R_i - R_i^{calc})^2/\delta R_i^2]$. The x-ray (Fig. 5) and neutron scattering-length-density depth profiles for the spin-up and spin-down polarizations (Fig. 6) are those for which the calculated reflectivities (solid curves in Figs. 2 and 3, respectively) minimized χ^2. The models for samples A, E, and F were refined relative to both the corresponding x-ray and neutron data at the same time; thus, the x-ray and neutron models share the same values for layer thickness and interface roughness. The values for the x-ray and neutron (nuclear) scattering length densities and the magnetizations for the layers are given in Table II.

The x-ray and neutron (nuclear) scattering-length densities deduced from the data were compared to those calculated for 25 iron and/or nickel-based compounds. The composition of layer 1 for samples E and F is most consistent with $Fe_2O_3 \cdot xH_2O$, $Fe(OH)_2$, $Fe(OH)_3$, or $Ni_3O_2(OH)_4$ (examples of oxyhydroxides or oxyhydrates). An oxyhydroxide layer was not required to fit the reflectivities of samples A through D; however, a subnanometer thick layer of such a compound might not have been detected in our x-ray and neutron reflectometry experiments. We note that the, additional layer (layer 1) was required to represent the additional modulation observed in the reflectivities of samples E and F (Fig. 2) that was not observed for samples A through D.

For the case of layer 2 for samples A through D only the calculated x-ray and neutron scattering-length densities of NiO (Bunsenite) were both consistent with experimental results (Table II). However, a two-phase mixture consisting of mostly NiO and a small amount (<10 at. %) of an iron oxide is also possible. For samples E and F, the x-ray and neutron scattering-length densities in layer 2 are larger than the densities obtained from samples A through D. Reduction of NiO would yield larger x-ray and neutron scattering-length densities. If metallic Ni were formed in layer 2, we would expect some ferromagnetism in layer 2. However, the neutron scattering data show that layer 2 is not likely ferromagnetic. The absence of ferromagnetism in layer 2 might be due to suppression of ferromagnetic ordering in such a thin film—at least to a magnitude below $M_s < 105$ kA/m (105 emu/cm^3), below which we do not have sufficient sensitivity to detect in these measurements. We note that the thickness of layer 2 was a free fitting parameter that was optimized in the models for all the samples. Nevertheless, the same fitted thickness of 1.5±0.3 nm was obtained for layer 2 for all samples, so the thickness of layer 2 (NiO) was not affected by annealing.

The x-ray and neutron (nuclear) scattering length densities of layer 3 of samples A through D are consistent with any one of four materials—FeO (Wüstite), α-Fe_2O_3 (hematite), Ni_2O_3, or $NiFe_2O_4$ (nickel ferrite). Unlike α-Fe_2O_3 and $NiFe_2O_4$, FeO (Wüstite) is not thermodynamically stable be-

TABLE III. Values of the chemical roughness of the oxide layer interfaces obtained with x-ray and neutron reflectometry.

Sample	Air-sample σ (nm)	Layers 1–2 σ (nm)	Layers 2–3 σ (nm)	Layer 3-Permalloy σ (nm)
A	0.32±0.05		0.39±0.05	0.48±0.05
B	0.36±0.05		0.18±0.05	0.59±0.05
C	0.31±0.05		0.15±0.05	0.67±0.05
D	0.18±0.05		0.13±0.05	1.0±0.1
E	0.57±0.05	0.34±0.05	0.06±0.05	0.50±0.05
F	1.0±0.1	0.36±0.05	0.05±0.05	0.35±0.05

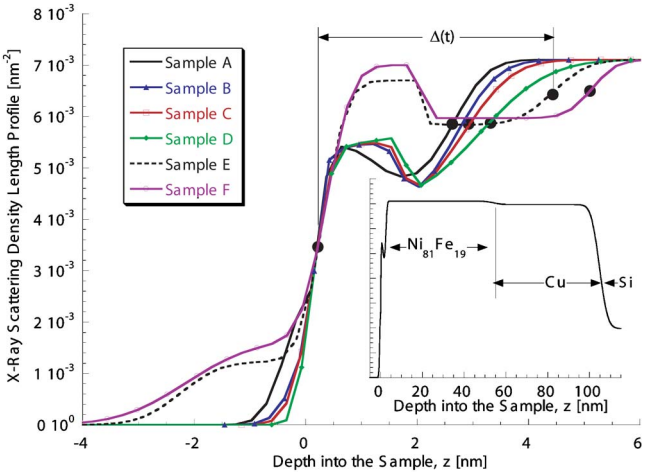

FIG. 5. (Color online) X-ray scattering-length density depth profiles of the samples near the air-sample interface are shown. The total thickness of the Ni oxide and Fe oxide layers is the distance between the inflection points (●). One inflection point is shown for the top surface ($z=0$) of the NiO layer. Others are shown for the interface between the iron-rich oxide and Permalloy layers, which progress to larger values of z with annealing time. The oxyhydroxide layer for the two most annealed samples is shown to the left of $z=0$ nm. The complete x-ray scattering density profile of the unannealed sample is shown in the inset. The profiles corresponding to the Permalloy, Cu, and Si portions of the sample (inset) are not statistically different for any of the samples.

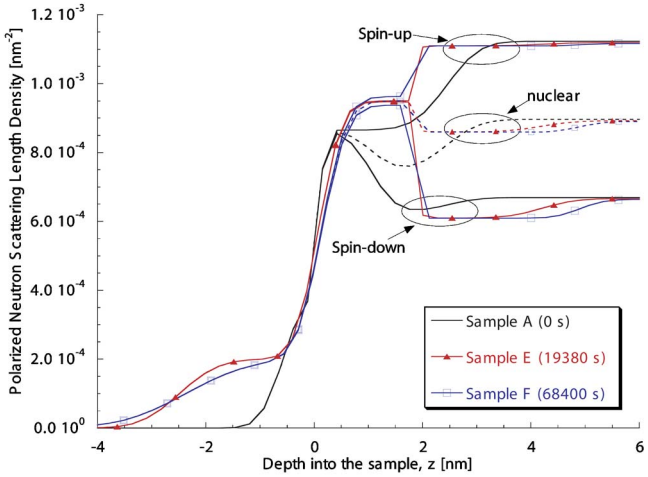

FIG. 6. (Color online) The spin-up and spin-down neutron scattering-length-density depth profiles (solid curves) of samples A, E, and F near the air-sample interface are shown. The neutron nuclear scattering-length-density profiles (dashed curves) are the averages of the spin-up and spin-down profiles. The separation of the spin-up and spin-down profiles is related to ferromagnetic order in the film and the moment of the magnetic species, corresponding to the depth into the sample plotted on the abscissa. The bifurcation at $z=0$ nm for the unannealed sample is due to the interdiffusion of Permalloy (the ferromagnetic material) with the oxide film (the nonferromagnetic material). The separation between depths 0 and 2 nm for sample F is not statistically significant.

low 843 K in the bulk; however, FeO has been previously observed in oxidized Fe films between layers of iron ferrite (Fe_3O_4, magnetite) and Fe.[18] Ni_2O_3 has been observed on the surfaces of Ni metal films[19–21] and as a product in electrochemical reactions of nickel and oxygen.[22]

No measurable net magnetic moment was observed for layer 3 in sample A. At room temperature, pure bulk α-Fe_2O_3 is an antiferromagnet; thus, α-Fe_2O_3 would exhibit no net magnetic scattering-length density, which is consistent with the neutron data. The magnetic structure of FeO (Wüstite) quenched to 12 K was observed to be antiferromagnetic by neutron diffraction.[23,24] Bulk $NiFe_2O_4$ is a ferrimagnet with a net magnetic scattering-length density that is larger than the upper limit of 105 emu/cm^3 established in this experiment. The magnetic properties of Ni_2O_3 are presently unknown.

In contrast to the case for sample A, layer 3 in samples E and F possesses moderate magnetization. The x-ray and neutron scattering-length densities for this layer are somewhat smaller than those in layer 2 (for these samples) or that of Permalloy. Reduction of the scattering-length densities can be achieved if layer 3 incorporates some oxygen or Fe at the expense of Ni—such as would be the case were layer 3 composed of a mixture of an oxide such as $NiFe_2O_4$ with Permalloy.

Bajorek *et al.*[25] concluded that the oxide of Permalloy is composed primarily of α-Fe_2O_3 based upon He-ion backscattering and x-ray fluorescence measurements. Antiferromagnetic ordering of an intentionally grown surface oxide has been inferred from both low-temperature hysteresis measurements and ferromagnetic resonance studies.[26,27] Such past studies argue for the presence of α-Fe_2O_3 in highly oxidized Permalloy films.

In contrast, Kitada[28] observed the formation of $NiFe_2O_4$ rather than α-Fe_2O_3 on Permalloy with *in situ* reflection high-energy electron diffraction. If the formation of a 1.5-nm-thick layer of NiO near the surface of Permalloy inhibits the migration of Fe to the sample surface, then the region beneath the NiO layer may be relatively rich in Fe compared to the concentration of Fe in Permalloy. The atomic density of iron in an iron-rich layer, arising from iron atoms "left behind" during the formation of NiO, can be related to the density of NiO, its thickness, and the thickness of the underlayer by $\rho_{Fe}=\rho_{NiO}(A_{Fe}/A_{NiO})(\Delta_{NiO}/\Delta_{layer\ 3})(19/81)$ through the atomic masses of the materials, A_{Fe} and A_{NiO}, and the ratio of 19/81 is the ratio of Fe to Ni in Permalloy ($Ni_{81}Fe_{19}$). In the case of sample D annealed for 3600 s, $\Delta_{NiO}/\Delta_{layer\ 3}=1.4$, so $\rho_{Fe}=2.5$ g/cm^3. This calculation assumes that every Fe atom previously mixed with Ni was left behind in layer 3, when layer 2 was formed as a pure phase of NiO. The upper limit on ρ_{Fe} is consistent with the density of Fe in $NiFe_2O_4$ where $\rho_{Fe}=2.4$ g/cm^3, but not consistent with the values of ρ_{Fe} in α-Fe_2O_3 or FeO, which are 3.7 and 4.6 g/cm^3, respectively.

The thickness Δ of the oxide between the NiO layer (where β_x achieves half the value for NiO; leftmost inflection point ● in Fig. 5) and the top of the Permalloy layer (equal to the average of β_x for the iron-rich oxide and Permalloy; Fig. 5) increases with annealing time t. The annealing time dependence of Δ is represented as $\Delta(t)$ in Fig. 7 and Table I. The shift of the oxide-Permalloy interface with annealing

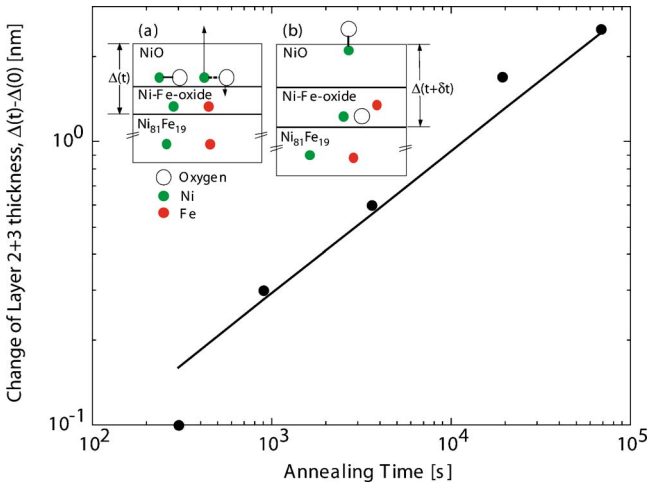

FIG. 7. (Color online) Change of the total thickness of layers 2 and 3 as a function of annealing time. Inset: The proposed method for growth of the oxide layer is shown. The thickness of the NiO layer is constant with time, while the thickness of the Fe oxide is governed by a parabolic growth rate.

time is given by $\delta\Delta(t)=\Delta(t)-\Delta(0)$ (Fig. 7). When these data are fitted to a diffusional growth model, where the increase in oxide thickness is governed by $\Delta(t)=\sqrt{K_p t}$, a parabolic rate constant of $K_p=10^{-18}$ cm^2 s^{-1} is obtained for annealing at 373 K. In addition to growth of the iron-rich oxide, the interface between layer 3 and the Permalloy film increases with annealing time up to 3600 s (Table III, samples A–D). An increase in roughness can be attributed to interdiffusion across the interface. If the interface becomes more diffuse with annealing, then oxygen might penetrate into the sample since the disassociation of Permalloy into Ni- and Fe-rich regions in the absence of oxygen is unlikely. (Fe is soluble in Ni at a concentration of 19 at. % Fe.) Diffusion in bulk NiO at moderate temperatures (above 1000 K) is known to occur via the exchange of Ni atoms with vacancies on the cation (Ni) sublattice.[29] At lower temperatures, diffusion occurs via the motion of Ni atoms along grain boundaries.[30,31] In either case, the transport of oxygen beneath the NiO layer might be limited by the rate at which NiO disassociates and/or the time required for Ni atoms to diffuse to the sample surface. The oxygen atom left behind after disassociation is able to bond to Ni or Fe atoms below the NiO layer. The growth of the oxide layer in this manner is shown schematically in Fig. 7 (inset). We note that the dramatic change (a decrease) in the roughness of the interface between layers 2 and 3 (see Table III and Fig. 6) occurs at the same time a change in both the chemical structure and magnetic property (i.e., the onset of strong ferromagnetism) of layer 3 is observed.

The second-harmonic polarization $P_p(2\omega)$ induced at a single ferromagnetic surface for p-polarized light may be broken into both magnetic and nonmagnetic components described by a magnetic second-order susceptibility $\chi_m^{(2)}$ and its nonmagnetic counterpart $\chi_{nm}^{(2)}$, i.e., $P_p(2\omega)=(\chi_{nm}^{(2)}+m\chi_m^{(2)})E_p^2(\omega)$, where m is the normalized magnetization along the transverse direction, and $E_p(\omega)$ is the electric field of the incident fundamental light. Thus, the power of the SHG signal is proportional to $|\chi_{nm}^{(2)}|^2+m^2|\chi_m^{(2)}|^2+2m|\chi_{nm}^{(2)}||\chi_m^{(2)}|\cos\phi$, where ϕ is the relative phase between the magnetic and nonmagnetic components of the susceptibility. For our SH-MOKE experiments, the normalized magnetization was switched between saturated states, i.e., $m=\pm 1$, in which case the measured signal I is simply $I_\pm=I_0(|\chi_{nm}^{(2)}|^2+|\chi_m^{(2)}|^2\pm 2|\chi_{nm}^{(2)}||\chi_m^{(2)}|\cos\phi)$. If we include the effect of bulk SHG from an adjacent oxide layer, the measured signal becomes $I_\pm=I_0(|\chi_{oxide}^{(2)}|^2+|\chi_{nm}^{(2)}|^2+|\chi_m^{(2)}|^2\pm 2|\chi_{nm}^{(2)}||\chi_m^{(2)}|\cos\phi)$, where the second-order susceptibility for the oxide layer is $\chi_{oxide}^{(2)}$ and we have assumed random phase between the bulk SHG in the oxide layer and the surface SHG from the magnetic layer. Since the average second-harmonic power I scales linearly with t (Fig. 4), $\chi_{oxide}^{(2)}$ follows a parabolic growth rate with annealing time such that $\chi_{oxide}^{(2)}\propto\sqrt{t}$ for $t<1$ h—a result consistent with the growth of the oxide layer thickness.[10,9]

Lee *et al.*[1] studied the formation of oxides on 100-nm-thick Permalloy films heated to temperatures between 433 and 523 K in the presence of 1 atm O_2. Using Auger electron spectroscopy and an ion beam to sputter material off the sample surface, Lee *et al.* identified the presence of $Ni(OH)_2$, NiO, and Fe_2O_3 on the Permalloy surface and obtained the oxide-layer thickness for each annealed sample. Extrapolating data for the parabolic rate constant shown in Fig. 6 of Ref. 1 to a temperature of 373 K, a value of $K_p\sim 1.3\times 10^{-18}$ cm^2 s^{-1} is obtained—a value that is consistent with one inferred from x-ray and neutron reflectometry of annealed films. Interestingly, the parabolic rate constants measured in both studies were found to be very similar despite the disparate availabilities of oxygen in the two experiments. Thus, formation of the Permalloy oxide is most likely controlled by diffusion of the metal species through grain boundaries and lattice defects and not the availability of oxygen at the Permalloy/air interface.

V. CONCLUSIONS

Under conditions of moderate heating (373 K) and low humidity, the oxide region formed on the surface of Permalloy thin films grows at a rate of $\sqrt{K_p t}$, where $K_p\sim 10^{-18}$ cm^2 s^{-1}. For annealing times of less than 1 h, the oxide region consists of a 1.5-nm-thick layer of NiO, whose thickness does not change with time, on top of an Fe-containing oxide layer that grows thicker with increasing annealing time. The NiO layer may limit the rate of oxidation of the Permalloy surface. If the oxide region is ferromagnetic, then it is only weakly so with a magnetization less than 105 kA/m. After 5 h of annealing, the Permalloy surface changes dramatically—consisting of a thick oxyhydroxide layer on top of layers of Ni or Fe metal or an alloy of these elements. Further, the oxide layer in contact with the Permalloy is ferromagnetic with a magnetic moment about 10% larger than that of the Permalloy film.

Modeling of SH-MOKE data[10,9] suggests that one of the surface oxides acts as a bulk source of second-harmonic generation. The $\sqrt{t}$ dependencies of $\chi_{oxide}^{(2)}$ and the Fe oxide layer thickness suggest that the Fe oxide layer (the oxide layer in contact with the Permalloy film) is the source of SHG that

did not depend upon magnetic field. Since the plausible oxides identified in the present study all exhibit a center of symmetry and therefore are incapable of bulk SHG in the electric-dipole limit, they may produce bulk SHG due to magnetic-dipole effects. *Ab initio* calculations of the magnetic-dipole SHG efficiency are difficult, and bulk SHG measurements are sparse for the magnetic oxides considered here, although α-Fe_2O_3 is confirmed to be a source of SHG.[32] Previous SHG experimental studies of antiferromagnetic Cr_2O_3—a material that lacks a center of symmetry in the magnetically ordered state—yielded significant SHG that was attributed to both electric- and magnetic-dipole sources of comparable magnitudes.[4] We note that Cr_2O_3 shares the same trigonal crystalline symmetry with α-Fe_2O_3; however, unlike Cr_2O_3, α-Fe_2O_3 has a center of symmetry in the magnetically ordered state.[33] We conclude that if α-Fe_2O_3 were the source of thickness-dependent SHG in the Permalloy annealing experiments, then SHG would necessarily result from the magnetic-dipole source term.[4]

ACKNOWLEDGMENTS

This work was supported by the U.S. Department of Energy, BES-DMS under Contract No. W-7405-Eng-36. The Manuel Lujan, Jr., Neutron Scattering Center is a national user facility funded by the U.S. Department of Energy, Office of Basic Energy Science. We are grateful to J. Dykes, formerly of Quantum MKQC, who generously provided the Permalloy samples used for this study. We are grateful to P. Yashar and S. Arnold for reviewing the manuscript.

*Present address: Department of Physics and Astonomy and USC NanoCenter, University of South Carolina, Columbia, SC 29208.

[1] W.-Y. Lee, G. Scherer, and C. R. Guarnieri, J. Electrochem. Soc. **126**, 1533 (1979).
[2] B. Koopmans, M. G. Koerkamp, T. Rasing, and H. van den Berg, Phys. Rev. Lett. **74**, 3692 (1995).
[3] H. A. Wierenga, M. W. J. Prins, D. L. Abraham, and Th. Rasing, Phys. Rev. B **50**, 1282 (1994).
[4] M. Fiebig, D. Froehlich, G. Sluyterman, and R. V. Pisarev, Appl. Phys. Lett. **66**, 2906 (1995).
[5] Y. R. Shen, *The Principles of Nonlinear Optics* (John Wiley and Sons, New York, 1984), pp. 86–93.
[6] R.-P. Pan, H. D. Wei, and Y. R. Shen, Phys. Rev. B **39**, 1229 (1989).
[7] T. M. Crawford, C. T. Rogers, T. J. Silva, and Y. K. Kim, IEEE Trans. Magn. **32**, 4087 (1996).
[8] T. M. Crawford, C. T. Rogers, T. J. Silva, and Y. K. Kim, IEEE Trans. Magn. **33**, 3598 (1997).
[9] T. M. Crawford, C. T. Rogers, T. J. Silva, and Y. K. Kim, Appl. Phys. Lett. **68**, 1573 (1996).
[10] T. J. Silva, T. M. Crawford, C. T. Rogers, and Y. K. Kim, in *Nonlinear Optics: Materials, Fundamentals, and Applications*, OSA Technical Digest Series Vol. 11 (Optical Society of America, Washington DC, 1996), pp. 299–301.
[11] L. G. Parratt, Phys. Rev. **95**, 359 (1954).
[12] M. R. Fitzsimmons and C. F. Majkrzak, in *Modern Techniques for Characterizing Magnetic Materials*, edited by Y. Zhu (Kluwer, Boston, 2005), pp. 107–152.
[13] G. P. Felcher, R. O. Hilleke, R. K. Crawford, J. Hanmann, R. Kleb, and G. Ostowski, Rev. Sci. Instrum. **58**, 609 (1987).
[14] C. F. Majkrzak, Physica B **221**, 342 (1996).
[15] M. R. Fitzsimmons, S. D. Bader, J. A. Borchers, G. P. Felcher, J. K. Furdyna, A. Hoffmann, J. B. Kortright, Ivan K. Schuller, T. C. Schulthess, S. K. Sinha, M. F. Toney, D. Weller, and S. Wolf, J. Magn. Magn. Mater. **271**, 103 (2004).
[16] S. Park, M. R. Fitzsimmons, X. Y. Dong, B. D. Schultz, and C. J. Palmstrøm, Phys. Rev. B **70**, 104406 (2004).
[17] H. Dosch, Phys. Rev. B **35**, 2137 (1987).
[18] R. J. Borg and G. J. Dienes, *An Introduction to Solid State Diffusion* (Academic Press, Boston, 1988), pp. 293–296.
[19] R. S. Conell, D. A. Corrigan, and B. R. Powell, Sol. Energy Mater. Sol. Cells **25**, 301 (1992).
[20] S. I. Shah, B. A. Doele, I. Weerasekera, and K. M. Unruh, Thin Solid Films **206**, 264 (1991).
[21] S. J. Bushby, T. D. Pope, B. W. Callen, K. Griffiths, and P. R. Norton, Surf. Sci. **256**, 301 (1991).
[22] T. P. Murphy and M. G. Hutchins, Sol. Energy Mater. Sol. Cells **39**, 377 (1995).
[23] H. Fjellvåg, F. Grønvold, S. Stølen, and B. Hauback, J. Solid State Chem. **124**, 52 (1996).
[24] K. Koike and T. Furukawa [Phys. Rev. Lett. **77**, 3921 (1996)] observed with spin-polarized electron spectroscopy evidence for ferromagnetic order in the top 0.2 nm of FeO. Neutron scattering does not normally have the surface sensitivity of the electron probe to detect magnetic order in such a thin layer. We note the thickness of layer 3 is about 2.0 nm.
[25] C. H. Bajorek, M.-A. Nicolet, and C. H. Wilts, Appl. Phys. Lett. **19**, 82 (1971).
[26] F. B. Hagedorn, J. Appl. Phys. **38**, 1362 (1967).
[27] C. E. Patton and C. H. Wilts, J. Appl. Phys. **38**, 3537 (1967).
[28] M. Kitada, J. Mater. Sci. **26**, 4150 (1991).
[29] A. Atkinson, R. I. Taylor, and A. E. Hughes, Philos. Mag. A **45**, 823 (1982).
[30] S. V. Kumari, M. Natarajan, V. K. Vaidyan, and P. Koshy, J. Mater. Sci. Lett. **11**, 761 (1992).
[31] S. Mitra, Mater. Sci. Eng., A **174**, 103 (1994).
[32] M. Fiebig (private communication).
[33] R. R. Birss, *Symmetry and Magnetism* (North-Holland, Amsterdam, 1964), pp. 131–134.